International Journal of Mechanical and Production Engineering Research and Development (IJMPERD)
ISSN (P): 2249-6890; ISSN (E): 2249-8001
Vol. 9, Issue 6, Dec 2019, 293–306

A TRAINED NEURAL NETWORK FOR THE PREDICTION OF OPTIMUM OPERATION MODE OF A STIRLING ENGINE

FATEMEH SOBHNAMAYAN, FARAMARZ SARHADDI & AMIN BEHZADMEHR

Research Laboratory of Renewable Energies and Electromagnetic Fluids, Department of Mechanical Engineering, University of Sistan and Baluchestan, Zahedan, Iran

ABSTRACT

In this paper, a prototype Stirling engine is fabricated and tested. In order to find the optimum operation mode of the engine, a neural network is trained and developed using the experimental data, which are obtained from the test of the engine. The trained neural network can predict the thermal efficiency of the Stirling engine for input parameters such as angular speed and gas chamber temperature. The neural network results are validated by the experimental data. Finally, the optimization of the thermal efficiency of the Stirling engine is carried out using the genetic algorithm. The results show that the neural network is a good tool for the prediction of the thermal efficiency of the Stirling engine. The optimum value of angular speed and gas chamber temperature obtained is 240.5 rpm and 489.5 K, respectively. Also, the maximum thermal efficiency of the Stirling engine is 31.05%.

KEYWORDS: Stirling Engine, Optimization, Neural Network & Genetic Algorithm

Received: Sep 17, 2019; **Accepted**: Oct 07, 2019; **Published**: Oct 26, 2019; **Paper Id.**: IJMPERDDEC201925

Original Article

1. INTRODUCTION

The world's largest renewable energy source is solar energy. “Solar Stirling engine is one of the main candidates for efficient use of the solar energy. The Stirling engine is a type of an external combustion engine and its agent fluid works in a closed cycle. The advantages of a Stirling engine include low emissions, low noise and vibration, use of different energy sources (fossil fuel, nuclear fuel and solar)” [1]. Concentrated parabolic dishes are commonly used to increase solar radiation on the heat source of a Stirling engine. Concentrated parabolic dishes increase thermal efficiency by raising operating temperature in the Stirling cycle. Common types of Stirling engines include alpha, beta and gamma. In the meantime, the gamma-type Stirling engine is more commonly used because of its higher thermal efficiency [1]. Therefore, the present study investigates the performance of a gamma-type Stirling engine. Robert Stirling invented and patented the Stirling hot air cycle in the 19th century [2]. Sanft in 1998 studied the thermodynamic performance of a Stirling engine [3]. He introduced thermal efficiency of the engine as a function of volume ratio, temperature ratio and heat recovery effectiveness. Kaushik and Kumar in 2000 analyzed a Stirling engine based on finite time thermodynamics [4]. They reported the maximum output power and thermal efficiency of 74.32 kW and 43.93%, respectively. Cinar et al. in 2005 tested a beta-type Stirling engine [5]. Their results showed that by increasing the heat in the hot source of the engine, the engine output power is increased. Parlak et al. in 2009 presented a model to predict the thermodynamic behavior of a gamma-type Stirling engine using a quasi-stationary flow model [6]. Cheng and Yu in 2010 developed a numerical model for a beta-type Stirling engine with a rhombic driving mechanism [7]. Their results show that the output power and thermal efficiency are highly dependent on geometric and physical parameters such as recovery length, spacing between crankshafts, crankshaft exit distance and hot source

temperature. Shendage et al in 2011 analyzed the features of a rhombic drive mechanism in a beta-type Stirling engine [8]. Their engine was able to produce an output power of 1.5 kW. Chen et al. in 2012 analyzed the thermal performance of a gamma-type Stirling engine [9]. Their results showed that the maximum output power of the engine and the thermal efficiency were 596 W and 36.3%, respectively. Duan et al. in 2013 analyzed the dynamic and thermodynamic analysis of a beta-type Stirling engine [10]. They showed that the medium-pressure power formula is the most appropriate way to estimate the output power of low temperature Stirling engines. Solmaz and Karabulut in 2014 introduced a new configuration of the beta-type Stirling engine with only one driving lever [11]. The results of their new engine performance compared to the engine with rhombic driving mechanism showed that the power of the lever engine was greater than that of the rhombic engine. Hooshang et al. in 2015 used a neural network to predict the performance of a gamma-type Stirling engine [12]. The simulation results from the neural network had an error less than 2% and also responded much faster than the usual thermodynamic codes. Xiao et al. in 2017 used computational fluid dynamics analysis (CFD) to determine the distribution of velocity, pressure, and temperature in the expansion chamber and compression chamber of a beta-type Stirling engine [13]. Then they optimized some of the relevant engine objective functions such as thermal efficiency, output power and current resistance loss. Their optimization results in a 2% increase in thermal efficiency and an increase of 80 W in output power. Barreto and Canhoto in 2017 carried out the dynamic and thermodynamic simulation of a solar Stirling dish system [14]. The main components of the system included a beta-type Stirling engine, a parabolic dish, a thermal receiver and an electric generator. The results of their analysis showed that the optimal value of dish concentration coefficient was 250 and the maximum overall efficiency was 10.41%. Çınar et al. in 2018 conducted an experimental study of the performance of an alpha-type Stirling engine [15]. They investigated the effect of air and helium working fluid on the engine performance in the pressure range of 1–4 bar and temperature range of 1000–100°C. Their results showed that the maximum output power of the engine is 30.7 W with helium gas at an angular speed of 437 rpm. Castro Caetano et al. in 2019 presented a new methodology for simulating a beta-type Stirling engine [16]. Their methodology consisted of combining Schmidt's first-order model and CFD simulation. The simulation output power of their new methodology has only 2.7% error with respect to the related experimental data.

In the present study, by designing and manufacturing a gamma-type Stirling engine, its experimental performance is investigated. To simulate the performance of a Stirling engine based on the experimental data, a relevant neural network is trained and developed. Finally, a genetic algorithm is used to find the optimal operation mode of the Stirling engine.

2. EXPERIMENTAL SETUP

“A prototype gamma-type Stirling engine is designed and fabricated. Figure 1 shows a picture and schematic view of the experimental setup of the gamma-type Stirling engine”.

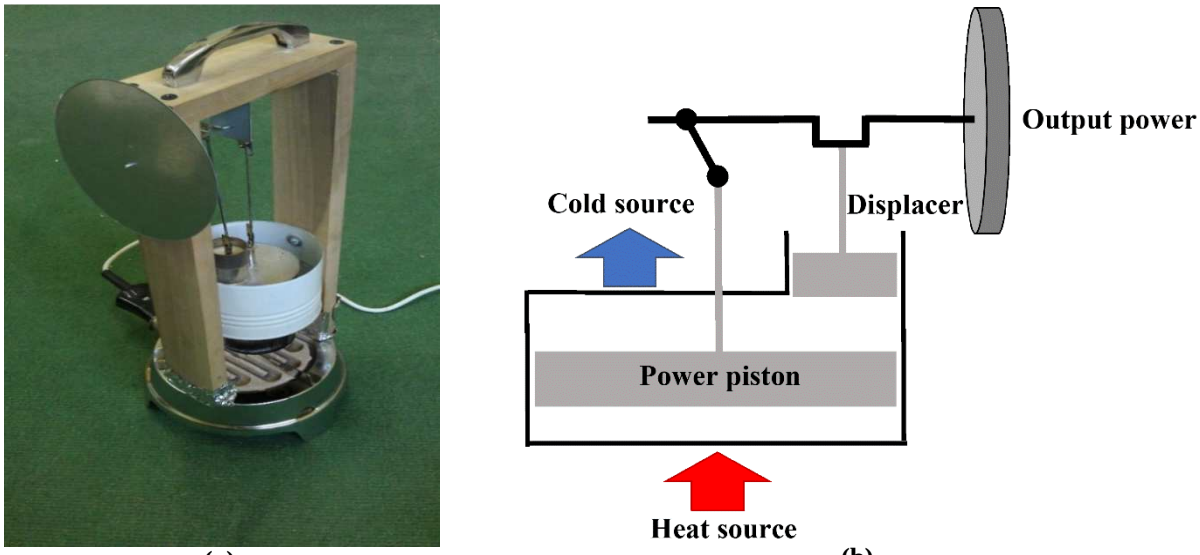

Figure 1: (a) "Picture of the Experimental Setup, (b) Schematic View of the Gamma-Type Stirling Engine".

The specifications of the experimental setup are given in Table 1.

Table 1: "The Specifications of the Experimental Setup"

Parameter	Value
Power piston diameter	7 cm
Displacer diameter	2.5 cm
Flywheel diameter	12 cm
Crank length	8 cm
Rod length	12 cm
Working fluid	air
Operating pressure	1 atm
The volume of heat section	192.4 cm^3
The volume of cold section	192.4 cm^3
Heat source power	200 W

A 200 W electrical heater with uniform power is used as a heat source for the Stirling engine during the course of experiments. In order to create various operating conditions, the different cooling fluids (air, water, and oil) are used in cold source. The measured parameters during the course of experiments include coolant fluid temperature (T_f), ambient temperature (T_a), gas chamber temperature (T_g), cylinder temperature (T_w) and angular speed of flywheel (ω). The measurement instruments and their precision are given in Table 2.

Table 2: "Uncertainty of Measurement Instrument"

Parameter	Instrument	Uncertainty
Coolant fluid and ambient temperature	Digital thermometers (Built-In-Thermometer −40..+110 °C)	±0.5°C
Gas chamber and cylinder temperature	Infrared thermometer (FLUKE-62)	±0.5°C
Angular speed of flywheel	Laser Tachometer (Benetech GM8905)	± 0.1 rpm

3. GOVERNING EQUATIONS

3.1 Experimental Calculations

In experimental calculations, "relations between input and output operating parameters of the Stirling engine is govern by the experimental setup. Figure 2 shows the thermodynamic control volume of the Stirling engine.

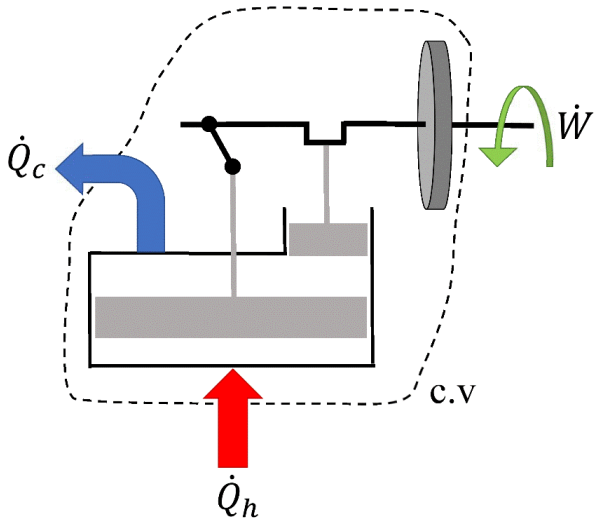

Figure 2: Thermodynamic Control Volume of the Stirling Engine

The general form of energy balance for the control volume of the Stirling engine is written as follows:

$$\dot{E}_{in} - \dot{E}_{out} - \dot{W} + \dot{E}_{gen} = \dot{E}_{st} \tag{1}$$

where $\dot{E}_{in}$, $\dot{E}_{out}$, $\dot{W}$, $\dot{E}_{gen}$ and $\dot{E}_{st}$ are the rate of input energy to the control volume, the rate of output energy of the control volume, shaft work rate, energy generation rate within the control volume and the rate of energy change in the control volume, respectively. Here $\dot{E}_{st}$ and $\dot{E}_{gen}$ is zero due to the steady state condition and no heat generation in the Stirling engine. An electrical heater supplies the rate of input energy to the control volume of the Stirling engine. Its power is kept constant due to the course of experiments.

$$\dot{E}_{in} = \dot{Q}_h = 200 \text{ W} \tag{2}$$

The rate of output energy of the control volume of the Stirling engine includes convective heat loss to coolant fluid and the increase of energy content of coolant fluid as follows:

$$\dot{E}_{out} = \dot{Q}_c = \dot{Q}_{conv} + \dot{Q}_{coolant} \tag{3}$$

$$\dot{Q}_{conv} = \bar{h}A(T_w - T_a) \tag{4}$$

$$\dot{Q}_{coolant} = mC\frac{\Delta T}{\Delta t} \tag{5}$$

where $\bar{h}$, A, m, C, ΔT and Δt are convective heat transfer coefficient of coolant fluid, surface area of cooling section, mass of coolant fluid, temperature increase of coolant fluid and time interval, respectively.

The convective heat transfer coefficient of coolant fluid is calculated as follows [17].

$$\bar{h} = \frac{k\overline{Nu}}{D} \tag{6}$$

$$\overline{Nu} = \left(0.825 + \frac{0.387 Ra^{\frac{1}{6}}}{\left(1 + \left(\frac{0.492}{Pr} \right)^{\frac{9}{16}} \right)^{\frac{8}{27}}} \right) \tag{7}$$

$$Ra = \frac{g\beta(T_w - T_a)}{\upsilon\alpha} \tag{8}$$

where $\overline{Nu}$, Ra, D, Pr, g, β, υ, k and α are average Nusselt number, Rayleigh number, diameter of gas chamber, Prandtl of coolant fluid, gravity acceleration, volume expansion coefficient of coolant, viscosity of coolant, conductivity and thermal diffusivity of coolant, respectively.

By substituting Equations (2)–(5) in Equation (1), an expression for the calculation of output power of the Stirling engine is obtained as follows:

$$\dot{W} = \dot{Q}_h - \dot{Q}_c = \dot{Q}_h - \bar{h}A(T_w - T_a) - mC\frac{\Delta T}{\Delta t} \tag{9}$$

The thermal efficiency of the Stirling engine is defined as follows:

$$\eta = \frac{\dot{W}}{\dot{Q}_h} = 1 - \frac{\bar{h}A(T_w - T_a) + mC\frac{\Delta T}{\Delta t}}{\dot{Q}_h} \tag{10}$$

In order to obtain the experimental data, 500 various experimental cases are created and measured by changing the conditions of the cold source of the Stirling engine. In order to show the calculation method of the experimental value of output power and thermal efficiency of the Stirling engine from the captured experimental data, a sample case of experimental data is given in Table 3.

Table 3: A Sample Case of the Measured Experimental Data

Parameter	Value
Coolant fluid	Water
The rate of input thermal energy	$\dot{Q}_h = 200$ W
Gas chamber temperature	$T_g = 503$ K
Ambient temperature	$T_a = 300$ K
The increase of coolant fluid temperature	$\Delta T = 8$ K
Angular speed	$\omega = 259$ rpm
Output power	$\dot{W} = 56.9$ W
Thermal efficiency	$\eta = 28.45\%$

Figure 3 shows the experimental value of thermal efficiency versus angular speed for the different value of the gas chamber temperature.

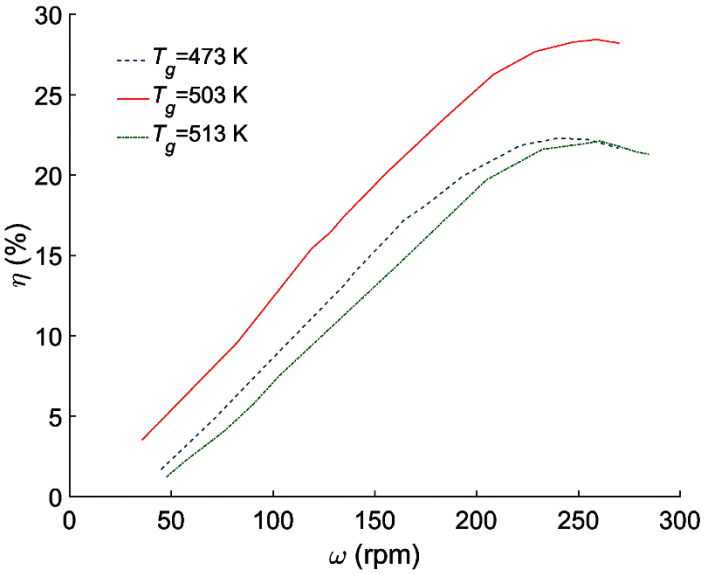

Figure 3: Experimental Value of Thermal Efficiency Versus Angular Speed for the different Value of the Gas Chamber Temperature.

3.2 Simulation by Neural Network

"The conventional simulation methods of the Stirling engine include the numerical solution of a nonlinear set of dynamic and thermodynamic equations. Usually, the solution of this nonlinear set is more complex and time-consuming. In the present study, a neural network is trained and developed to simulate the Stirling engine performance. The input data to neural network is angular speed and gas chamber temperature and the output parameter from neural network is the thermal efficiency. A neural network with the help of artificial intelligence concepts constitutes the relation between input and output data. Neural network training is carried out by the experimental data. When a neural network is trained and developed it able to predict the output parameters with a good accuracy" [18, 19]."A neural network includes an input layer, an output layer and several hidden layers. The information of the trained network is stored in these layers [20]. In order to evaluate the trained neural network, some regression criteria are used as follows" [20].

Matching coefficient:

$$R^2 = 1 - \left(\frac{\sum_{i=1}^{N} (a_i - p_i)^2}{\sum_{i=1}^{N} a_i^2} \right) \tag{11}$$

Mean square error:

$$RMSE = \sqrt{\frac{1}{N} \sum_{i=1}^{N} (a_i - p_i)^2} \tag{12}$$

Coefficient of variation:

$$COV = \frac{RMSE}{\sum_{i=1}^{N} a_i} \times 100 \tag{13}$$

where N, a and p represent the number of data, the experimental data and predicted data, respectively. The structure of the neural network of the present study consists of four hidden layers and an input layer and output layer (Figure 4). This neural network is constructed by sigmoid functions neurons for hidden layers and linear neurons for the input and output layer.

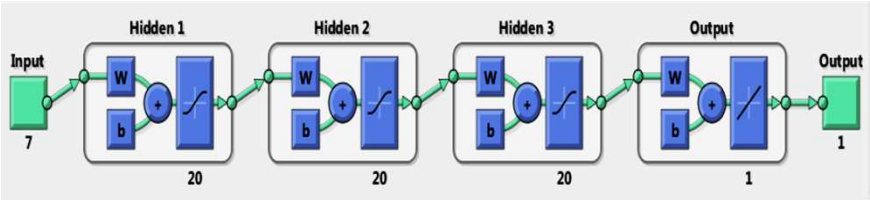

Figure 4: Structure of the Neural Network of the Present Study.

The neural network of the present study is trained and developed using 500 experimental data of the experimental setup of the Stirling engine. The number of neurons in hidden layers is determined by regression analysis, which is given in Table 4.

Table 4: "Number of Neurons in Hidden Layers"

Number of Neurons	R^2	*RMSE*
5	0.9679	0.182364
15	0.9745	0.107397
30	0.9831	0.092741
45	0.9984	0.071312
60	0.9995	0.0611568
75	0.9995	0.0611568
90	0.9995	0.0611568

According to Table 4, after the neurons number of 60 no change in R^2 and *RMSE* can be seen. Therefore, the neural network structure of the present study consists of 7 neurons in the input layer, 60 neurons in the first, second and third hidden layers, one neuron in the fourth hidden layer and one neuron in the output layer (7-20-20-20-1-1).

In order to train and develop the neural network, the experimental data of Figure 3 for input parameters of angular speed and gas chamber temperature and the output parameter of thermal efficiency is used. The convergence of neural network of the present study is shown in Figure 5.

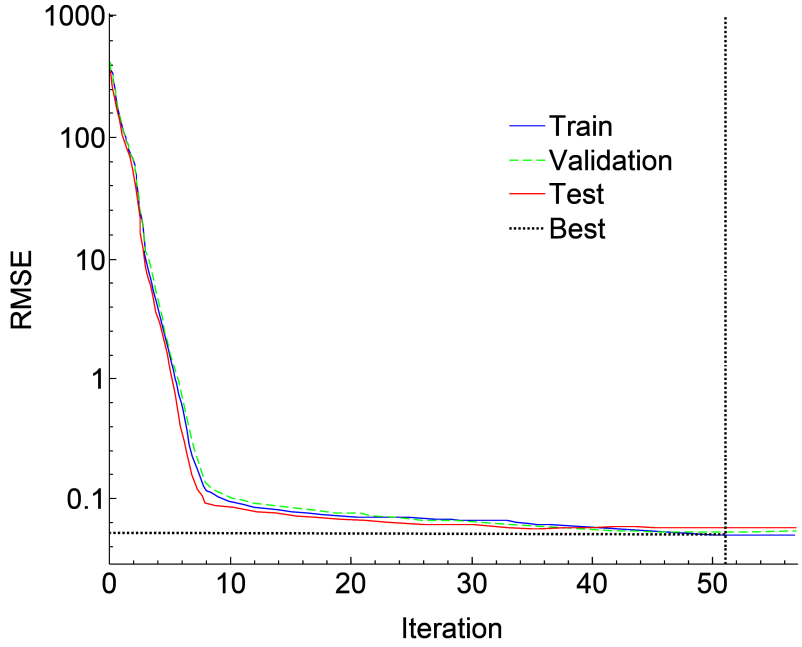

Figure 5: Convergence Graph of the Neural Network of the Present Study.

Matching coefficient and mean square error values for the network was 0.99 and 0.053, respectively.

4. VALIDATION

In order to validate the trained and developed neural network, a comparison is carried out between the simulation results of the neural network and the experimental data of Figure 3. This comparison is given in Figure 6.

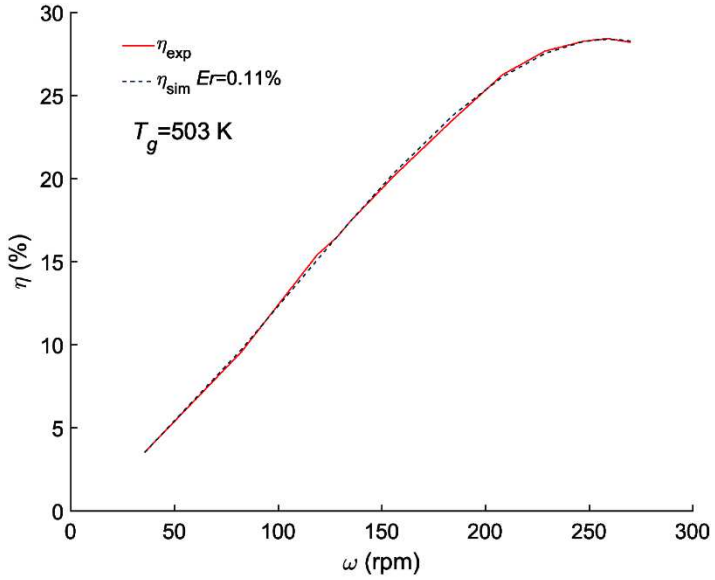

Figure 6: "Validation of the Simulation Results of the Neural Network"

The error between the experimental data and the simulation results of the neural network is calculated by the average relative error as follows:

$$Er = \frac{1}{n}\sum_{i=1}^{n}\left|\frac{X_{\exp,i} - X_{sim,i}}{X_{\exp,i}}\right| \times 100 \tag{14}$$

where X is the value of experimental or simulated data, and n represents the number of experimental data. According to Figure 6, the average relative error between the experiment and simulation is 0.11%. This implies that the developed neural network can accurately predict the performance of the Stirling engine.

5. FORMULATION OF THE OPTIMIZATION PROBLEM

In order to find the optimum operation mode of the Stirling engine, an optimization problem can be defined as follows:

$$\begin{cases} \text{Maximize } \eta = f(\omega, T_g) \\ \text{subject to} \\ 50 \le \omega \le 300 \text{ rpm} \\ 473 \le T_g \le 513 \text{ K} \end{cases} \tag{15}$$

The objective function is the thermal efficiency of the Stirling engine and decision variables include the angular speed and the gas chamber temperature. The genetic algorithm (GA) of optimization toolbox of MATLAB software is used for the maximization of the objective function.

6. RESULTS

The optimization results of the Stirling engine is given in Table 5.

Table 5: Optimization Results of the Stirling Engine

Optimum Decision Variable	Maximized Objective Function
$\omega_{opt} = 240.5$ rpm	$\eta_{max} = 31.05\%$
$T_{g,opt} = 489.5$ K	

It can be observed from Table 5 that if the design parameters of the Stirling engine are chosen equal to the optimum values, then the thermal efficiency of the Stirling engine will reach to a maximum of 31.05%. Furthermore, the corresponding output power at the optimum point is 62.1 W.

Figure 7 shows the variation of the thermal efficiency of Stirling engine versus changes in the gas chamber temperature and the angular speed.

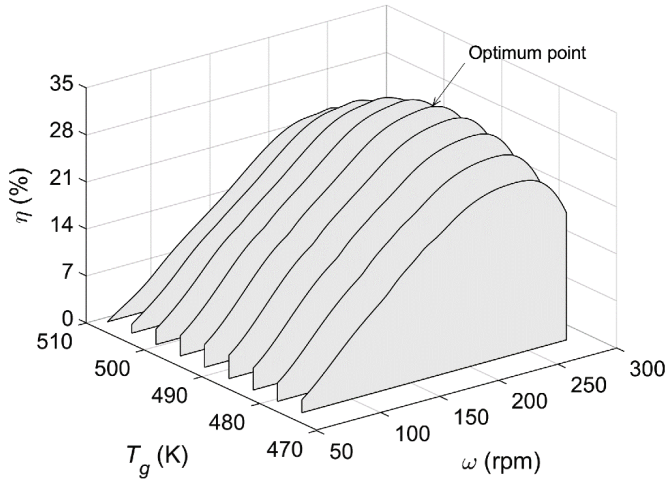

Figure 7: Variation of the Thermal Efficiency of Stirling Engine versus Changes in the Gas Chamber Temperature and the Angular Speed.

As can be seen in Figure 7, "the related surface has a global maximum point. The coordinate of this maximum point corresponds to the optimum values of gas chamber temperature and angular speed". Outside the optimal point, the thermal efficiency drops. Decreasing the gas chamber temperature before the optimum point means less heat entering the Stirling engine. Increasing the gas chamber temperature after the optimum point results in increased heat losses from the Stirling engine. Therefore, the maximum efficiency is only at the optimum point.

In order to show the accuracy of the optimum point of thermal efficiency in the following figures, the variation of angular speed and gas chamber temperature are plotted separately.

In Figure 8, the variation of the thermal efficiency of Stirling engine versus the angular speed for the optimum gas chamber temperature is drawn.

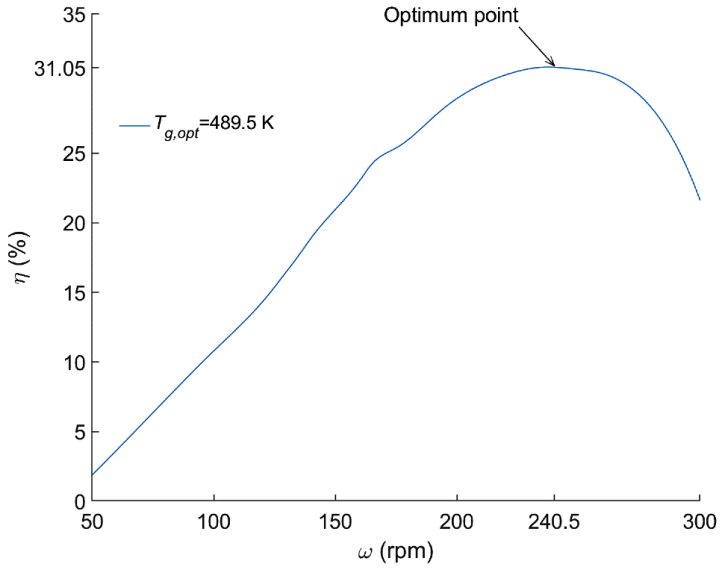

Figure 8: "Variation of the Thermal Efficiency of Stirling Engine versus the Angular Speed for the Optimum Gas Chamber Temperature".

According to Figure 8, "the maximum thermal efficiency of the Stirling engine is equal to 31.05% for the optimal angular speed of 240.5 rpm. By increasing the angular speed higher than 240.5 rpm, the Stirling engine goes to the instability condition and its efficiency drops".

Figure 9 shows the variation of the thermal efficiency of Stirling engine versus the changes of gas chamber temperature for the optimum angular speed.

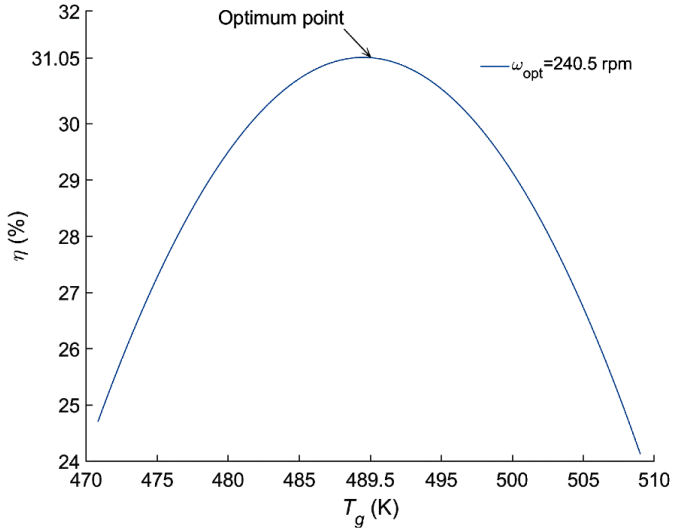

Figure 9: "Variation of the Thermal Efficiency of Stirling Engine Versus the Changes of Gas Chamber Temperature for the Optimum Angular Speed".

According to Figure 9, increasing the gas chamber temperature means increasing the heat input to the Stirling engine. By increasing the gas chamber temperature to the optimum value of 489.5 K, the thermal efficiency increases. However, after the optimum point, the thermal efficiency decreases due to the increase in thermal losses from the Stirling engine.

7. CONCLUSIONS

In the present study, a Stirling engine was designed and fabricated. Some experimental data were taken from the engine. Based on the experimental data a neural network was developed and trained. The neural network results were optimized by genetic algorithm to find the optimal operation mode of Stirling engine. The results show that the neural network is a suitable and accurate tool for predicting the performance of the Stirling engine. If the Stirling engine is working at optimum mode, its efficiency increases.

NOMENCLATURE

A (m^2)	Surface area of cooling section
a	Experimental data
$C\left(\frac{J}{kg.K}\right)$	Specific heat capacity of coolant fluid
COV	Coefficient of variation
D (m)	Gas chamber diameter
$\dot{E}$ (W)	Energy rate
Er (%)	Average relative error

$g\ \left(\frac{\mathrm{m}}{\mathrm{s}^2}\right)$	Gravity acceleration
$\overline{h}\ \left(\frac{\mathrm{W}}{\mathrm{m}^2.\mathrm{K}}\right)$	Convective heat transfer of coolant fluid
i	Counter parameter
$k\ \left(\frac{\mathrm{W}}{\mathrm{m.K}}\right)$	Thermal conductivity of coolant fluid
m (kg)	Mass of coolant fluid
n	Number of experimental data
N	Number of data
$\overline{Nu}$	Nusselt number
p	Predicted data
Pr	Prandtl of coolant fluid
$\dot{Q}_c$ (W)	Thermal energy rate in cold source
$\dot{Q}_{conv}$ (W)	Convective heat loss to coolant fluid
$\dot{Q}_{coolant}$ (W)	Increase of energy content of coolant fluid
$\dot{Q}_h$ (W)	Thermal energy rate in hot source
R^2	Matching coefficient
Ra	Rayleigh number
$RMSE$ (%)	Mean square error
T (K)	Temperature
t (s)	Time
$\dot{W}$ (W)	Shaft work
X	Experimental or simulated parameter

Greek symbols

$\alpha\ \left(\frac{\mathrm{m}^2}{\mathrm{s}}\right)$	Thermal diffusivity of coolant fluid

$\beta\left(\frac{1}{\mathrm{K}}\right)$	Thermal diffusivity of coolant fluid
Δ	Difference in temperature and time
η (%)	Thermal efficiency
$\upsilon\left(\frac{\mathrm{m}^2}{\mathrm{s}}\right)$	Viscosity of coolant fluid
$\omega\ (\mathrm{rpm})$	Angular speed

Subscripts

a	Air
exp	Experimental
f	Coolant fluid
g	Gas chamber
gen	generation
in	Inlet
opt	Optimum
out	Outlet
sim	Simulated
st	Stored
w	Cylinder wall

REFERENCES

1. *E. Papadopoulou, Photovoltaic industrial systems, an environmental approach, Springer, New York; 2011.*
2. *G. Walker, Stirling engines, Oxford University Press, New York, 1980.*
3. *J. R. Senft, Theoretical limits on the performance of Stirling engines, International Journal of Energy Research, 22, 991–1000, 1998.*
4. *S. C. Kaushik, S. Kumar, Finite time thermodynamic analysis of endoreversible Stirling heat engine with regenerative losses, Energy, 25, 989–1003, 2000.*
5. *C. Cinar, S. Yucesu, T. Topgul, M. Okur, Beta-type Stirling engine operating at atmospheric pressure, Applied Energy, 81, 351–357, 2005.*
6. *Padmanaban, S., & William, M. L. (2016). A Nonparametric Discriminant Variable-Elimination Algorithm for Classification to Two Populations. International Journal of Applied Mathematics and Statistical Sciences, 5(6), 7–16.*
7. *M. Parlak, Thermodynamic analysis of a gamma type Stirling engine in non-ideal adiabatic conditions, Renewable Energy,*

34(1), 266–273, 2009.

8. *C. H. Cheng, Y. J. Yu, Numerical model for predicting thermodynamic cycle and thermal efficiency of a beta-type Stirling engine with rhombic-drive mechanism, Renewable Energy, 35, 2590–25601, 2010.*
9. *D. J. Shendage, S. B. Kedare, S. L. Bapat, An analysis of beta type Stirling engine with rhombic drive mechanism, Renewable Energy, 36(1), 289-297, 2011.*
10. *C. L. Chen, C. E. Ho, H. T. Yau, Performance analysis and optimization of a solar powered Stirling engine with heat transfer considerations, Energies, 5, 3573-3585, 2012.*
11. *C. Duan, C. Sun, Sh. Shu, G. Ding, Combined dynamic and thermodynamic analysis of a β type Stirling engine, International Conference on Sustainable Energy Technologies, Hong Kong, 2013.*
12. *H. Solmaz, H. Karabulut, Performance comparison of a novel configuration ofbeta-type Stirling engines with rhombic drive engine. Energy Conversion and Management, 78, 627–633, 2014.*
13. *Mengistu, A. D., & Alemayehu, D. M. (2016). Robot for visual object tracking based on artificial neural network. International Journal of Robotics Research and Development (IJRRD), 6(1), 1–6.*
14. *M. Hooshang, R. AskariMoghadam, S. AlizadehNia, M. Tale Masouleh, Optimization of Stirling engine design parameters using neural networks, Renewable Energy, 74, 855–866, 2015.*
15. *G. Xiao, U. Sultan, M. Ni, H. Peng, X. Zhou, Sh. Wang, Zh. Luo, Design optimization with computational fluid dynamic analysis of β-type Stirling engine, Applied Thermal Engineering, 113, 87–102, 2017.*
16. *G. Barreto, P. Canhoto, Modelling of a Stirling engine with parabolic dish for thermal to electric conversion of solar energy, Energy Conversion and Management, 132, 119–135, 2017.*
17. *C. Çınar, F. Aksoy, H. Solmaz, E. Yılmaz, A. Uyumaz, Manufacturing and testing of an a-type Stirling engine, Applied Thermal Engineering, 130, 1373–1379, 2018.*
18. *B. Castro Caetano, I. Figueiredo Lara, M. Ungaretti Borges, O. R. Sandoval, R. Molina Valle, A novel methodology on beta-type Stirling engine simulation using CFD, Energy Conversion and Management, 184, 510–520, 2019.*
19. *Y. Xuan, Q. Li, Investigation on convective heat transfer and flow features of nanofluids, Journal of Heat Transfer, 125(1), 151–155, 2003.*
20. *Equbal, A., Sood, A. K., Ansari, A. K., & Equbal, A. (2017). Optimization of process parameters of FDM part for minimiizing its dimensional inaccuracy. International Journal of Mechanical and Production Engineering Research and Development, 7(2), 57–65.*
21. *H. Xie, L. Liu, F. Ma, H. Fan, Performance prediction of solar collectors using artificial neural networks, International Conference on Artificial Intelligence and Computational Intelligence, Shanghai, China, 2009.*
22. *K. L. Du, M. N. S Swamy, Neural networks and statistical learning. Springer Science & Business Media, 2013.*
23. *A. S. Kalogirou, Artificial neural networks in renewable energy systems applications: a review, Renewable and Sustainable Energy Reviews, 5, 373–401, 2001.*